

Carbon dioxide column abundances at the Wisconsin Tall Tower site

R. A. Washenfelder¹, G.C. Toon², J-F. Blavier², Z. Yang¹, N.T. Allen³, P.O. Wennberg¹, S.A. Vay⁴,
D.M. Matross³, B.C. Daube³

¹California Institute of Technology, Pasadena, California, USA

²NASA Jet Propulsion Laboratory, California Institute of Technology, Pasadena, California, USA

³Harvard University, Cambridge, Massachusetts, USA

⁴NASA Langley Research Center, Hampton, Virginia, USA

Abstract

We have developed an automated observatory for measuring atmospheric column abundances of CO₂ and O₂ using near-infrared spectra of the sun obtained with a high spectral resolution Fourier Transform Spectrometer (FTS). This is the first dedicated laboratory in a new network of ground-based observatories named the Total Carbon Column Observing Network. This network will be used for carbon cycle studies and validation of spaceborne column measurements of greenhouse gases. The observatory was assembled in Pasadena, California, and then permanently deployed to northern Wisconsin during May 2004. It is located in the heavily forested Chequamegon National Forest at the WLEF Tall Tower site, 12 km east of Park Falls, Wisconsin. Under clear sky conditions, ~0.1% measurement precision is demonstrated for the retrieved column CO₂ abundances. During the Intercontinental Chemical Transport Experiment – North America and CO₂ Boundary-layer Regional Airborne Experiment campaigns in summer 2004, the DC-8 and King Air aircraft recorded eight in situ CO₂ profiles over the WLEF site. Comparison of the integrated aircraft profiles and CO₂ column abundances shows a small bias (~2%) but an excellent correlation.

1. Introduction

In the last two decades, numerous studies [e.g. *Gurney et al.*, 2002; *Rayner et al.*, 1999; *Tans et al.*, 1990] have combined in situ measurements of CO₂ obtained from a global network of surface sites [*GLOBALVIEW-CO2*, 2005] with global transport models to estimate regional-scale surface exchange of CO₂. Although the surface measurements are highly accurate, their limited spatial coverage and proximity to local sources and sinks make these estimates quite sensitive to the errors in the transport model (e.g. vertical mixing), particularly for sites located in the continental interior. In particular, because the surface fluxes and vertical transport are correlated on diurnal and seasonal timescales, errors in transport fields are aliased into the inferred exchange term as so-called "rectifier" effects [*Denning et al.*, 1996; *Gurney et al.*, 2002].

Precise and accurate CO₂ column measurements can complement the existing in situ network and provide information about CO₂ exchange on larger geographic scales. Unlike the near-surface volume mixing ratio (VMR), the column integral of the CO₂ profile is not altered by diurnal variations in the height of the boundary layer. As a result, it exhibits less spatial and temporal variability than near-surface in situ data, while retaining information about surface fluxes [*Gloor et al.*, 2000]. Because few CO₂ column measurements are available, understanding of their potential information content has been largely limited to simulations [*Rayner and O'Brien*, 2001; *Olsen and Randerson*, 2004]. These studies show that CO₂ column measurements at carefully selected sites could be effective in constraining global-scale carbon budgets [*Rayner and O'Brien*, 2001].

Three recent analyses of near-infrared FTS solar spectra obtained by Fourier Transform Spectrometers (FTS) demonstrate that column-averaged CO₂ VMRs can be retrieved with high precision [*Yang et al.*, 2002; *Dufour et al.*, 2004; *Warneke et al.*, 2005]. The near-infrared spectral region is an appropriate observational choice for several reasons: (i) it is near the peak of the solar Planck function, expressed in units of photons/s/m²/sr/cm⁻¹, maximizing signal-to-noise; (ii)

retrievals from O₂ absorption lines in the near-infrared spectral region provide an internal standard; (iii) highly sensitive uncooled detectors are available for this region. For these reasons, the near-infrared region has also been chosen by several space-based column observatories, including the Orbiting Carbon Observatory (OCO), the Scanning Imaging Absorption Spectrometer for Atmospheric Chartography (SCIAMACHY), and the Greenhouse Gases Observing Satellite (GOSAT).

Most of the existing FTS instruments from the Network for the Detection of Stratospheric Change (NDSC) [*Kurylo and Solomon, 1990*] are not well suited for measurement of CO₂ and other greenhouse gases. Most NDSC sites are located at high altitude to facilitate stratospheric measurements. To understand the sources and sinks of greenhouse gases, however, observatories should be located at low altitude. In addition, the existing NDSC sites are optimized for observations of the mid-infrared spectral region, with KBr beamsplitters, aluminum optics, and mid-infrared detectors. Although many trace atmospheric constituents have fundamental vibrational-rotational absorptions in the mid-infrared spectral region, the near-infrared spectral region is a better choice for measuring CO₂ and other greenhouse gases.

The Total Carbon Column Observing Network is a new network of ground-based FTS sites. We describe the first dedicated laboratory in this network. This is an automated FTS observatory developed for highly precise, ground-based solar absorption spectrometry in the near-infrared spectral region. Atmospheric column abundances of CO₂, CH₄, CO, N₂O, H₂O, HDO, O₂, and HF can be retrieved from the observed near-infrared spectral region. The observatory was assembled in Pasadena, California and then deployed to Park Falls, Wisconsin during May 2004. We compare the column CO₂ results with integrated in situ aircraft profiles, and present the CO₂ column values for May 2004 – October 2005. Readers interested in these results may wish to skip the detailed instrumental description in Section 2 and proceed directly to Section 3.

2. Instrumentation

2.1. Bruker 125HR Spectrometer

Solar spectra are acquired at high spectral resolution using a Bruker 125HR FTS housed in a custom laboratory (Figure 1). The Bruker 125HR has been substantially improved over its predecessor, the Bruker 120HR. One important improvement is the implementation of the interferogram sampling method described by *Brault* [1996], that takes advantage of modern 24-bit delta-sigma analog-digital converters to improve the signal-to-noise ratio.

The spectrometer described here has been optimized for measurements in the near-infrared spectral region, with gold-coated optics and a CaF₂ beamsplitter with broad-band coating. Interferograms are simultaneously recorded by two uncooled detectors. Complete spectral coverage from 3,800 – 15,500 cm⁻¹ is obtained by simultaneous use of an InGaAs detector (3,800 – 12,000 cm⁻¹) and Si-diode detector (9,500 – 30,000 cm⁻¹) in dual-acquisition mode, with a dichroic optic (Omega Optical, 10,000 cm⁻¹ cut-on). A filter (Oriel Instruments 59523; 15,500 cm⁻¹ cut-off) prior to the Si diode detector blocks visible light, which would otherwise be aliased into near-infrared spectral domain. The observed spectral region includes absorption bands of CO₂, CH₄, CO, N₂O, H₂O, HDO, O₂, and HF. Spectra from the Si-diode detector are not analyzed in this work, but are useful for comparison with OCO and other future satellite instruments measuring the $b^1\Sigma_g^+(v=0) \leftarrow X^3\Sigma_g^-(v=0)$ O₂ transition (A-band) between 12,950 and 13,170 cm⁻¹. For the spectra obtained here, we use a 45 cm optical path difference and a 2.4 mrad field of view, yielding an instrument line shape that has a full-width at half-maximum of 0.014 cm⁻¹. This is sufficient to fully resolve individual absorption lines in the near-infrared. The input optics uses an off-axis parabolic mirror that is the same type as the collimating mirror. Hence the external field of view is also 2.4 mrad, and the instrument accepts only a small fraction of the 9.4 mrad solar disk. The beam diameter

is stopped down to 3.5 cm to reduce the saturation of the detectors and signal amplifiers. Figure 2a shows a typical spectrum, acquired in 110 s, with signal-to-noise ratios of $\sim 900:1$ and $\sim 500:1$ for the InGaAs and Si diode detectors, respectively. The observed intensity is the product of the solar Planck function with the instrument response.

To maintain stability of the optical alignment, the internal temperature of the spectrometer is controlled between 28 – 30° C. To reduce acoustic noise and eliminate refractive inhomogeneities, the internal pressure is maintained at less than 2 hPa using a Varian TriScroll 300 scroll pump. The spectrometer is evacuated once per day, before sunrise, and has a leak rate less than 2 hPa day⁻¹. The instrument lineshape is monitored using narrow HCl lines in the first overtone band ($\nu_0 = 5882 \text{ cm}^{-1}$). A 10 cm cell with 30' wedged Infrasil windows containing 5.1 hPa of HCl gas is permanently mounted in the source compartment, prior to the entrance field stop wheel, as shown in Figure 1b. Due to space constraints, the sample compartment typically supplied with the 125HR is not used.

2.2. Laboratory and Other Instrumentation

The 125HR spectrometer is mounted inside a modified $6.1 \times 2.4 \times 2.6$ m steel shipping container. The container is equipped with an air conditioning and heating wall unit, power (110 VAC and 208 VAC), lights, and telephone connection. The interior of the container is insulated with 9.0 cm of R19 fiberglass covered with 0.32 cm thick aluminum sheet. These materials were chosen to minimize outgassing that may otherwise interfere with spectral observations.

The optical assembly (solar tracker) that transfers the direct solar beam from the roof of the container to the FTS was purchased from Bruker Optics. It consists of a servo-controlled assembly with two gold-coated mirrors that rotate in azimuth ($0^\circ - 310^\circ$) and elevation ($-5^\circ - +90^\circ$). The solar tracker has two operational modes: pointing to the calculated solar position and active servo-controlled tracking. Initially, the solar tracker is pointed toward the calculated solar ephemeris. This

position is typically within 0.3° of the actual solar position, with error attributed to the alignment and leveling of the solar tracker. The solar beam is directed down through a hole in the laboratory roof, which is sealed with an 11.5 cm diameter wedged CaF_2 window. Inside the laboratory, a small fraction of the incoming solar beam is focused onto a Si quadrant detector located at the entrance to the spectrometer. The solar tracker then uses the quadrant detector signal for active tracking of the sun, with a manufacturer-specified tracking accuracy of 0.6 mrad. Three heaters on the base of the solar tracker activate when the temperature drops below 5°C , to prevent damage to the optics and electronics.

The solar tracker is housed in a fiberglass telescope dome, manufactured by Technical Innovations, Inc. in Barnesville, Maryland. The dome is constructed of industrial grade fiberglass, with a $1.0 \text{ m} \times 1.3 \text{ m}$ oval base. The wide shutter opening allows unobstructed views from the horizon to 5° beyond zenith. The dome is bolted to the container roof, which is reinforced with eight 6.4 cm thick steel tubes welded to the frame, and covered with a 0.64 cm thick steel plate. This stabilizes the solar tracker and prevents vibrations that may degrade spectral quality and flexing of the container roof which may degrade the solar tracker alignment.

A Setra Systems, Inc. Model 270 pressure transducer ($\pm 0.3 \text{ hPa}$), is mounted inside the container, with an input tube at $\sim 2 \text{ m}$ outside. Accurate knowledge of the pressure is important for evaluating of the accuracy of the retrieved O_2 columns. In addition, synoptic surface pressure variations of $\pm 10 \text{ hPa}$ ($\pm 1\%$) would overwhelm the changes in the total CO_2 column that we wish to observe. The calibration of the pressure sensor is checked periodically by comparison to a Fortin mercury manometer (Princo Instruments, Model 453) mounted in the laboratory as an absolute standard. In addition, the temperature of the Setra pressure transducer is monitored for evidence of bias. A weather station mounted at $\sim 5 \text{ m}$ includes sensors for air temperature ($\pm 0.3^\circ \text{C}$), relative

humidity ($\pm 3\%$), solar radiation ($\pm 5\%$ under daylight spectrum conditions), wind speed ($\pm 0.5 \text{ m s}^{-1}$), wind direction ($\pm 5^\circ$), and the presence of rain.

A small network camera (Stardot Technologies) with a fisheye lens (2.6 mm focal length) is positioned on the roof of the laboratory. The dome, solar tracker, weather station, and a wide view of the sky are visible within the field of view of the camera. This allows us to remotely monitor the operation of the equipment and verify weather conditions.

Accurate knowledge of the time is critical in calculating the solar zenith angle (SZA), which is necessary to convert retrieved atmospheric slant column abundances into vertical column abundances. We use a high-precision GPS satellite receiver with a network time server (Masterclock NTP100-GPS) to maintain time synchronization of the Bruker 125HR.

2.3. Data Acquisition and Instrumental Automation

The laboratory equipment consists of the 125HR spectrometer, scroll pump, solar tracker, dome, weather station, NTP-GPS satellite time receiver, network camera, heaters (for 125HR, solar tracker, and scroll pump), temperature sensors, current and voltage sensors, and uninterruptible power supply (UPS). Each of these components is monitored and/or controlled with an integrated CPU board (Hercules, Diamond Systems) and an additional custom-built control board. The Hercules board includes four serial ports, used for communication with the solar tracker, dome, weather station, and modem. The Hercules board also includes 32 wide-range analog inputs for monitoring temperatures, voltage, currents, and the pressure of the scroll pump. Five digital I/O lines of the Hercules board are used to command power to the solar tracker, dome, modem, FTS, and the FTS reset line. The FTS, network camera, NTP-GPS satellite time receiver, and UPS are IP-addressable and are commanded within the local area network.

The operating system chosen for the Hercules computer is QNX (QNX, Kanata, Ontario), a realtime, multitasking, multiuser, POSIX-compliant operating system for the Intel family of microprocessors. QNX was selected due to its stability and because its simple message-passing method of inter-process communication allows the acquisition and control functions of the data acquisition software to be separated into a number of logically discrete processes.

Throughout the night, the acquisition software records weather and housekeeping data. When the calculated solar elevation angle reaches 0° , the scroll pump is commanded on and the FTS is evacuated to 0.5 hPa. Following the pumping sequence, the dome opens and the solar tracker points to the calculated solar ephemeris. If the solar intensity is sufficient (45 W m^{-2}), the solar tracker begins active tracking of the sun and the FTS begins acquisition of solar interferograms. The specific acquisition parameters, including the field stop diameter, detector gains, scanner velocity, and optical path difference, are set in software. Typically, each scan requires 110 seconds to complete and consists of a single-sided interferogram with 45 cm optical path difference recorded at 7.5 kHz laser fringe rate. Forward and reverse interferograms (with the moving mirror traveling away from and toward the fixed mirror) are acquired in sequence. Throughout each scan, the solar intensity measured by the solar tracker quadrant sensor is recorded at 0.5 Hz. Since only spectra acquired under stable solar intensity are suitable for atmospheric retrievals, the standard deviation of the solar intensity is later used to evaluate spectral quality. Forward and reverse interferograms are analyzed separately to maximize the number of unobstructed scans. Acquisition of solar interferograms continues as long as the solar intensity is sufficient for active tracking of the sun. If the weather station detects rain, then the dome closes and spectral acquisition ceases until weather conditions improve. When the calculated solar elevation reaches 0° at the end of the day, the dome is closed.

Each night, interferograms recorded during the day are copied onto a removable hard disk. Overnight analysis software performs a Fourier transform to produce spectra from the interferograms, and performs preliminary atmospheric column retrievals. These results are then emailed to Pasadena to monitor performance. At two month intervals, the removable hard disk is manually replaced with an empty one. The full disk is mailed to Pasadena for analysis and archiving. This is necessary because only dial-up internet access is available at the WLEF site. The operational data rate is $\sim 50 \text{ GB month}^{-1}$.

3. Measurement Site

The FTS observatory was assembled and tested in Pasadena, California, and deployed to northern Wisconsin during May 2004. The laboratory is located 25 m south of the WLEF television tower site (45.945 N, 90.273 W, 442 m above sea level) in the Chequamegon National Forest, 12 km east of Park Falls, Wisconsin (pop. 2800). The region is heavily forested with low relief, and consists of mixed northern hardwoods, aspen, and wetlands. Boreal lowland and wetland forests surround the immediate research area. The Chequamegon National Forest was extensively logged between 1860 and 1920, but has since regrown.

This site was chosen because the National Oceanic and Atmospheric Administration Earth Systems Research Laboratory (NOAA ESRL) and other organizations conduct extensive in situ measurements at the WLEF tower, facilitating intercomparison between the column and boundary layer measurements. Monitoring began in October 1994, when WLEF was added as the second site in the Tall Tower program. CO₂ concentrations are measured continuously at six levels on the 447 m tower [Zhao *et al.*, 1997; Bakwin *et al.*, 1995]. Fluxes of CO₂, water vapor, virtual temperature, and momentum are monitored at three levels [Berger *et al.*, 2001; Davis *et al.*, 2003]. In addition,

NOAA ESRL conducts weekly flask sampling [Komhyr *et al.*, 1985] and monthly aircraft profiles which collect flask samples between 0.5 km and 4 km [Bakwin *et al.*, 2003].

4. Data Analysis

In this work, spectra are analyzed using a non-linear least-squares spectral fitting algorithm (GFIT) developed at the Jet Propulsion Laboratory. Atmospheric absorption coefficients are calculated line-by-line for each gas in a chosen spectral window, and are used together with the assumed temperature, pressure, and VMR profile in the forward model to calculate the atmospheric transmittance spectrum. This is compared with the measured spectrum and the VMR profiles are iteratively scaled to minimize the RMS differences between the calculated and measured spectra. The theoretical instrument lineshape, verified from fits to low-pressure HCl gas cell lines, is used in calculating the forward model. Figure 2b shows a measured spectrum and the fitted result, for a region with strong CO₂ lines.

The atmosphere is represented by 70 levels in the forward model calculation. Pressure- and temperature-dependent absorption coefficients are computed for each absorption line at each level. Profiles of temperature and geopotential height are obtained from the NOAA Climate Diagnostics Center (CDC), with 17 pressure levels from 1000 to 10 hPa and 1° × 1° geographic resolution. At pressures less than 10 hPa, climatological profiles of temperature and geopotential height are used. Measured surface pressure is used to define the lowest model level.

We retrieve CO₂ and O₂ in three bands: O₂ 0–0 $a^1\Delta_g^- X^3\Sigma_g^-$ ($\nu_0 = 7882 \text{ cm}^{-1}$); CO₂ (14°1) – (00°0) ($\nu_0 = 6228 \text{ cm}^{-1}$); and CO₂ (21°2) – (00°0) ($\nu_0 = 6348 \text{ cm}^{-1}$). These will be referred to as the O₂ 7882 cm⁻¹, CO₂ 6228 cm⁻¹, and CO₂ 6348 cm⁻¹ bands. Retrievals in these three bands require accurate spectroscopic parameters for O₂, CO₂, H₂O, and solar lines. The HITRAN 2004 linelist parameters [Rothman *et al.*, 2005] were found to be deficient at the high accuracies that we require.

In HITRAN 2004, the O₂ 7882 cm⁻¹ band has severe errors in strengths for low J lines and errors in widths for high J lines; the CO₂ 6228 cm⁻¹ and 6348 cm⁻¹ bands have errors in line positions, air-broadened widths, and pressure shifts.

We have adopted improved line parameters for the O₂ 7882 cm⁻¹ retrievals, including line strengths from PGOPHER model results [Newman *et al.*, 2000], air-broadened widths [Yang *et al.*, 2005], and temperature-dependent air-broadened widths [Yang *et al.*, 2005]. In addition, we have made two empirical corrections to minimize temperature and airmass dependence of the O₂ retrieval: (i) The air-broadened width values [Yang *et al.*, 2005] have been increased by 1.5%. (ii) The temperature-dependence of the air-broadened width values [Yang *et al.*, 2005] have been increased by 10% to bring them into better agreement with measurements by Newman *et al.* [2000]. Both of these empirical corrections are within the reported measurements uncertainties. Four recent laboratory studies report the integrated O¹⁶O¹⁶ 7882 cm⁻¹ band strength as $3.166 \pm 0.069 \times 10^{-24}$ cm molecule⁻¹ [Lafferty *et al.*, 1998], $3.10 \pm 0.10 \times 10^{-24}$ cm molecule⁻¹ [Newman *et al.*, 1999] (all O₂ isotopes), $3.247 \pm 0.080 \times 10^{-24}$ cm molecule⁻¹ [Cheah *et al.*, 2000], and $3.210 \pm 0.015 \times 10^{-24}$ cm molecule⁻¹ [Newman *et al.*, 2000]. Because the Newman *et al.* [2000] PGOPHER model shows good agreement with our atmospheric fitting retrievals, we have also adopted the Newman *et al.* [2000] integrated band strength.

In addition to the discrete lines of the O₂ 7882 cm⁻¹ band, there is an underlying continuum absorption caused by collision-induced absorption. Based on laboratory measurements [Smith and Newnham, 2000; Smith *et al.*, 2001], we generated a model of collision-induced absorption which includes separate contributions from O₂-O₂ and O₂-N₂ collisions. Although the collision-induced absorption is included in the line-by-line calculation to improve estimation of the continuum, only the discrete 7882 cm⁻¹ O₂ lines are used in the computation of the O₂ column amount.

We have used updated line parameters for the CO₂ 6228 cm⁻¹ and 6348 cm⁻¹ band line strengths, air-broadened widths, and pressure shifts based on recent work by Bob Toth [*in preparation*, 2006]. We have also adopted updated H₂O line parameters for the 5000 – 7973 cm⁻¹ region [Toth, *private communication*, 2005]. These new linelists were found to give superior spectral fits to our atmospheric spectra. The solar linelist for all near-infrared spectral retrievals is derived from disk-center solar spectra recorded at Kitt Peak (31.9 N, 116 W, 2.07 km).

For O₂, the assumed a priori VMR profiles are constant with altitude. For CO₂, the assumed a priori VMR profiles vary seasonally in approximate agreement to model output from *Olsen and Randerson* [2004]. We have examined the sensitivity of the column CO₂ retrieval to different reasonable a priori functions, including a profile which is constant with altitude, and found that the effect on retrieved column CO₂ is $\leq 0.1\%$.

5. Column O₂ and CO₂

The consistency between retrieved column O₂ and measured surface pressure is an important test of instrumental stability. O₂ is well-mixed in the atmosphere, with a dry-air VMR of 0.2095. This provides an internal standard that can be used to check the short-term and long-term precision of the FTS column retrievals. As described in Section 3, surface pressure at the Park Falls site is recorded at 1 Hz using a calibrated Setra 270 pressure sensor. The calibrated accuracy of this sensor is ~0.3 mb, which corresponds to an uncertainty of ~0.03% in the surface pressure. For the May 2004 – October 2005 spectra, retrieved column O₂ is consistently $2.27 \pm 0.25\%$ higher than the dry pressure column (where the dry pressure column is equal to the observed surface pressure converted to a column density minus the retrieved H₂O column). This error exceeds both the uncertainty in the dry pressure column and the reported 0.5% uncertainty in the integrated O¹⁶O¹⁶ 7882 cm⁻¹ band strength of 3.21×10^{-24} cm molecule⁻¹ $\pm 0.015 \times 10^{-24}$ cm molecule⁻¹ [Newman *et al.*, 2000].

However, the $\sim 4\%$ spread in recent measurements of the integrated $\text{O}^{16}\text{O}^{16}$ 7882 cm^{-1} band strength (Section 4) suggests that this discrepancy may fall within the uncertainty of the laboratory measurements. In this analysis, the retrieved O_2 columns have been reduced by 2.27% to bring the retrievals into agreement with the known atmospheric concentration of O_2 . Figure 3a shows O_2 retrievals for airmasses between 2 and 3 (SZA 60 – 70 deg) plotted as a function of the dry pressure column. Throughout this work, “airmass” refers to the ratio of the slant column to the vertical column and is approximately equal to the secant of the SZA; when the sun is directly overhead, the SZA is 0 deg and the airmass is 1.0. The residuals are shown in the upper panel of Figure 3a.

Figure 3b shows the time series of O_2 VMR, calculated from column O_2 / dry pressure column. Results are not shown for 8 May 2005 – 14 Jul 2005, due to an instrumental error in solar pointing. Much of the scatter in Figure 3b can be attributed to error in the linestrengths and the air-broadened widths that cause the O_2 retrievals to vary with temperature and airmass. However, the systematic increase in O_2 VMR over time ($\sim 0.3\%$) is larger than (and of opposite sign to) the seasonal changes in O_2 VMR. Coincident changes in HCl concentration retrieved from the calibration cell are also observed. During May 2004 – October 2005, the reflectivity of the gold-coated solar tracker mirrors slowly degraded due to a manufacturing flaw. This reduced the measured solar intensity by approximately 60% in the near-infrared spectral region. We believe that the errors observed in the O_2 and HCl retrievals may be caused by this signal loss, coupled with non-linearity in the response of the InGaAs detector. Studies are underway to quantify this error and remove its influence on the retrievals.

Column retrievals of CO_2 from the 6228 cm^{-1} and 6348 cm^{-1} bands show high precision and repeatability. Observations of column CO_2 during one clear day and one partly cloudy day in August 2004 are shown in Figure 4a. Figure 4b shows the column O_2 retrievals during the same time period. Spectra have been discarded as obstructed by clouds if the solar intensity measured by the quadrant

detector fluctuated by more than 5% rms during the recording of an interferogram. The mean and standard deviation of the CO₂ columns measured during a one-hour clear observation period around local noon (24 individual spectra) on 14 Aug 2004 is $7.7235 \pm 0.0078 \times 10^{21} \text{ cm}^{-2}$ and $7.7406 \pm 0.0074 \times 10^{21} \text{ cm}^{-2}$ respectively for the 6228 cm⁻¹ and 6348 cm⁻¹ CO₂ bands. This precision of ~0.1% is typical for column CO₂ obtained under clear sky conditions in Park Falls. However, the 6228 cm⁻¹ and 6348 cm⁻¹ band CO₂ retrievals differ by ~0.2% in absolute column CO₂. This is attributed to errors in spectroscopic parameters for linestrengths and air-broadened linewidths. Observations on 15 Aug 2004 during partly cloudy conditions show greater variability in Figures 4a and 4b, even after filtering for the standard deviation of the solar radiance to remove spectra that are significantly obstructed by clouds. Column-average CO₂ VMR can be calculated from retrieved CO₂ column, according to

$$f_{CO_2, avg} = \frac{column_{CO_2}}{total \ dry \ column} \quad (1)$$

There are two methods for calculating the total dry column:

$$total \ dry \ column = \frac{P_s}{m_{air} g} - column_{H_2O} \quad (2)$$

$$total \ dry \ column = \frac{column_{O_2}}{0.2095} \quad (3)$$

where P_s is surface pressure, m is mean molecular mass, and g is the density-weighted gravitational acceleration. In Park Falls, the column H₂O correction in (2) is a maximum of 0.6%.

Using (3) will improve the precision of the column-average CO₂ VMR (f_{CO_2}) if scatter in the column abundances is common to both the CO₂ and O₂. Common scatter could arise from errors in the spectra, such as instrumental lineshape or detector non-linearity, or from errors in the calculated slant path due to uncertainty in the surface pressure or SZA. However, dividing by column O₂ will increase the random scatter (since column O₂ is typically noisier than P_s) and will introduce spectroscopic linelist errors from the O₂ region, such as temperature- and airmass-dependence, into the column-average CO₂ VMR. In addition, the systematic changes in column O₂ observed over time in Figure 3b are likely due to detector non-linearity. However, this systematic error is expected to affect the CO₂ and O₂ column retrievals similarly, and can be eliminated from the column-average CO₂ VMR by using (1) and (3).

Column-average CO₂ VMR calculated via (2) and (3) is shown in Figures 4c and 4d. Comparing Figures 4c and 4d, the greatest improvement in scatter is seen on the partly cloudy day (15 Aug 2004). The major sources of scatter on cloudy days are error in the solar pointing and variation in intensity during the scan, which affect the CO₂ and O₂ retrievals similarly. Dividing column CO₂ by column O₂, rather than dry pressure column, therefore improves the precision, especially on partly cloudy days. A comparison of the results is shown in Table 1.

Table 1. Mean and standard deviation during 1-hour observational period around local noon.

	Column CO ₂ (10 ²¹ cm ⁻²)	Column CO ₂ / dry surface pressure (ppmv)	0.2095 × column CO ₂ / column O ₂ (ppmv)
Clear day (14 Aug 04) 6228 cm ⁻¹ band	7.7235 ± 0.0078	376.46 ± 0.30	376.55 ± 0.26
Clear day (14 Aug 04) 6348 cm ⁻¹ band	7.7406 ± 0.0074	377.29 ± 0.28	377.38 ± 0.22
Cloudy day (15 Aug 04) 6228 cm ⁻¹ band	7.707 ± 0.058	375.8 ± 2.8	375.48 ± 0.82
Cloudy day (15 Aug 04) 6348 cm ⁻¹ band	7.724 ± 0.055	376.7 ± 2.7	376.35 ± 0.68

6. Comparison of FTS Column and Integrated Aircraft Profiles

The Intercontinental Chemical Transport Experiment – North America (INTEX-NA) and CO₂ Boundary-layer Regional Airborne Experiment (COBRA) campaigns provided an opportunity

to calibrate the column CO₂ measurements on an absolute scale relative to the standardized network of in situ measurements. As the difference between CO₂ 6228 cm⁻¹ and 6348 cm⁻¹ column retrievals in Figure 4a demonstrates, results from each of the CO₂ bands are precise, but not sufficiently accurate. This is attributed to remaining limitations in the available spectroscopic parameters.

The NASA DC-8 and University of Wyoming King Air measured in situ CO₂ during profiles over the WLEF Tall Tower site during summer 2004, using well-calibrated, mature in situ CO₂ sensors. Onboard the DC-8, dry CO₂ VMR was measured at 1 Hz using a modified LI-COR model 6252 infrared gas analyzer [Vay *et al.*, 2003; Anderson *et al.*, 1996]. In-flight calibrations were performed at 15 minute intervals using standards traceable to the WMO Central CO₂ Laboratory. Onboard the King Air, similar 1 Hz measurements were performed using a modified LI-COR model 6251 [Daube *et al.*, 2002]. In-flight calibrations were performed with standards traceable to the Carbon Dioxide Research Group at the Scripps Institute of Oceanography and NOAA ESRL. In-flight calibrations show that the typical long term flight-to-flight precision of this technique is better than ±0.1 ppmv [Daube *et al.*, 2002].

The aircraft CO₂ profiles can be integrated with respect to pressure for direct comparison with FTS column CO₂. Mathematically, this is found by combining the definition of the column integral

$$column_{CO_2} = \int_{Z_s}^{\infty} f_{CO_2} n dz \quad (4)$$

with the hydrostatic equation

$$dz = \frac{-dp}{gm_{air} n} \quad (5)$$

to yield

$$column_{CO_2} = \int_0^{P_s} \frac{f_{CO_2}}{gm_{air}} dp \quad (6)$$

where f is the atmospheric mixing ratio, g is gravitational acceleration, m_{air} is the mean molecular mass, n is the number density, p is pressure, P_s is surface pressure, z is height, and Z_s is the surface height. The atmospheric mixing ratio of CO_2 is defined as

$$f_{CO_2} = f_{CO_2,dry} (1 - f_{H_2O}) \quad (7)$$

where $f_{CO_2,dry}$ is the dry-air CO_2 vmr, measured by in-situ instruments. Combining equations (6) and (7) gives

$$column_{CO_2} = \int_0^{P_s} \frac{f_{CO_2,dry}}{gm_{air,dry} \left(1 + \frac{m_{H_2O}}{m_{air,dry}} \left(\frac{f_{H_2O}}{1 - f_{H_2O}} \right) \right)} dp \quad (8)$$

Integrated column CO_2 from (8) can be divided by the total column from (2) to yield the column-average CO_2 VMR.

Eight unique aircraft profiles were measured on five dates during 2004: 12 Jul, 14 Jul, 15 Jul, 14 Aug, and 15 Aug. The first profile of the series, shown in Figure 5a, was a descending spiral by the NASA DC-8 from 10.0 km to 0.7 km. Because the aircraft has a limited altitude range, it is necessary to make assumptions about CO_2 and H_2O in the upper troposphere and stratosphere when using (8) to find integrated column CO_2 . The tropopause pressure is determined from the NOAA

CDC assimilated temperature profile. The median CO₂ value measured in the free troposphere is assumed to extend from the aircraft ceiling to the tropopause. Above the tropopause, the assumed CO₂ profile is taken from an in situ balloon profile (35 N, 104 W) recorded over Fort Sumner, New Mexico during September 2004. The balloon profile of CO₂ as a function of altitude is coordinate-transformed into CO₂ as a function of potential temperature (θ), using simultaneous temperature and pressure measurements. For the aircraft profile, θ is calculated from the NOAA CDC assimilated temperature data. CO₂ is assumed to be well-mixed in the planetary boundary layer between the surface and the 0.7 km floor of the aircraft profile. This is confirmed by in situ measurements on the Tall Tower. The CO₂ profile shown in Figure 5b is integrated with respect to pressure to find column CO₂. The assumed CO₂ profile above the aircraft ceiling contributes the greatest uncertainty to the integration, and we have attributed a generous uncertainty of ± 2 ppmv to this portion of the profile.

Figure 5d shows the FTS column-average CO₂ recorded during a two-hour period which brackets the aircraft profile. These profiles were performed at airmass 1.1 – 2.0 (SZA 25 – 60 deg). The column data is not continuous, because intermittent cloud prevented the acquisition of solar spectra. The 45-minute period of the aircraft profile is indicated. The averaging kernel for the FTS CO₂ retrievals during this period is shown in Figure 5c. The shape of the averaging kernel is typical for a uniformly mixed, moderately strong absorber fitted by a non-linear least-squares profile-scaling retrieval. To accurately compare the FTS column-average CO₂ and integrated aircraft profile, it is necessary to weight the aircraft profile by the FTS averaging kernel [Rodgers and Connor, 2003]. Because the averaging kernel varies slightly with airmass, a separate averaging kernel is calculated for each aircraft overpass.

Comparison of the eight integrated aircraft profiles with the FTS CO₂ columns is shown in Figure 6. There is a linear relationship between the integrated aircraft columns and the retrieved FTS columns. The slope relationships differ for the two CO₂ bands, with values of 1.0216 and 1.0240 for

CO₂ 6228 cm⁻¹ and CO₂ 6348 cm⁻¹ respectively. The standard deviation of the fitting residuals is 0.39 ppmv and 0.42 ppmv for the two bands. The slope relationships from Figure 6 can be used to correct the FTS CO₂ columns, bringing them into absolute agreement with the calibrated in situ network.

7. Error Analysis for Column-Average CO₂ VMR

The column-average CO₂ VMR calculated according to $0.2095 \times \text{column CO}_2 / \text{column O}_2$ is affected by three main sources of error:

1. Measurement precision

As discussed in section 5, the standard deviation of column CO₂ / column O₂ during a one hour period is better than 0.1% under clear sky conditions and ~0.2% under partly cloudy conditions. Repeatability of the measurement is not a significant source of error.

2. Spectroscopic errors

As discussed in section 5, the retrieved O₂ columns were reduced by 2.27% to bring them into agreement with the dry surface pressure. Although this correction falls outside the reported uncertainty of the ¹⁶O¹⁶O 7882 cm⁻¹ integrated band strength, we believe that it is likely attributed to an error in the line strengths or air-broadened width parameters.

The absolute accuracy of the CO₂ retrievals was calibrated by comparison to integrated aircraft profiles, resulting in a correction of 1.0216 and 1.0240 for the CO₂ 6228 cm⁻¹ and 6348 cm⁻¹ bands. The standard deviation of the fitting residuals is 0.39 ppmv and 0.42 ppmv, or approximately 0.1%. The aircraft profiles were performed with the sun at airmass 1.1 – 2.0 (SZA 25 – 60 deg), and the column-average CO₂ VMR is now well-calibrated for these values. However, this does not

calibrate the column-average CO₂ VMRs at higher airmass. A 1% change in the air-broadened widths results in a CO₂ VMR change of ~0.2% (± 0.8 ppmv) at airmass 3 and ~0.6% (± 2.3 ppmv) at airmass 12. These parameters are not sufficiently constrained by current spectroscopic linelists, leaving this as a significant source of systematic error which can be correlated with airmass, time of day, and temperature.

3. Systematic instrumental changes over time

As described in section 5, retrieved O₂ VMR increased by ~0.3% during the observation period. Because this increase is seen for O₂ retrievals from the InGaAs detector in the 7882 cm⁻¹ band, and not for O₂ retrievals from the Si diode detector in the 13095 cm⁻¹ A-band, we believe that this is due to detector nonlinearity and can be corrected. We expect that this error affects the CO₂ and O₂ retrievals similarly, but for now assume that the column CO₂ / column O₂ ratio may also have a systematic error of 0.3% over the observation period.

The measurement precision of ~0.1% under clear sky and ~0.2% under partly cloudy conditions does not affect the accuracy of the measurements. However, spectroscopic errors introduce a systematic bias which depends on airmass. We have calibrated the FTS column retrievals at airmass 1.1 – 2.0 during Jul – Aug 2004, and expect that the absolute accuracy at these airmasses has been maintained within 0.3% throughout the subsequent data record.

8. Column-average CO₂ VMR during May 2004 – October 2005

Applying the slope corrections from section 6 allows the FTS column-average CO₂ VMR to be compared directly to in situ CO₂ measurements. Column-average CO₂ VMR, corrected in this manner, is shown in Figure 7a, together with in situ CO₂ measurements from 30-m and 396-m on the

Tall Tower. The in situ CO₂ measurements are influenced by the diurnal rectifier effect, which is caused by the overnight decrease in the height of the planetary boundary layer. During the day, CO₂ surface fluxes are diluted within a thicker boundary layer, while CO₂ surface fluxes at night are concentrated near the surface. The column-average CO₂ VMR is minimally influenced by the diurnal rectifier effect. Summertime drawdown in CO₂ is observed in both the in situ and column measurements.

The seasonal cycle of column-average CO₂ VMR observed at Park Falls during May 2004 – Oct 2005 is shown as daily averages for airmasses between 2 – 4 (SZA 60 – 75 deg) in Figure 7b. In situ CO₂ measurements from the Tall Tower are shown as daily averages between 16:00 – 20:00 UT (10:00 – 14:00 CST). As expected, the variation of CO₂ is muted in the column, as compared to surface measurements, on all timescales. During May 2004 – May 2005, the observed peak-to-peak variation of column-average CO₂ VMR is approximately 13 ppmv, with an average value of 376.2 ppmv. Comparing column-average CO₂ retrievals observed in September and October during 2004 and 2005, we calculate a secular increase of 1.8 ppmv yr⁻¹. After accounting for this, we infer a peak-to-peak seasonal amplitude of 11 ppmv for Park Falls. These results are higher than model results by *Olsen and Randerson* [2004], which predict a mean seasonal column CO₂ amplitude of 7 – 8 ppmv in Wisconsin. This difference could potentially arise from an error in the model predictions, due to uncertainty in the specifications of surface fluxes or errors in the parameterization of mixing. Alternatively, the difference could be caused by differences between the assumed meteorology and emission inventories included in the MATCH model.

9. Conclusions

We have deployed an automated solar observatory to Park Falls, Wisconsin. Near-infrared solar absorption spectra have been acquired continuously since May 2004. Short-term and long-term

precision are evaluated by the repeatability of column retrievals within a day and by the comparison of column O₂ with surface pressure measurements. The precision of retrieved column CO₂ under clear-sky conditions is ~0.1%, as determined by the 1 σ variability of retrievals recorded within one hour. Under partly cloudy conditions, the CO₂ column precision is much worse, but can be improved by dividing column CO₂ by column O₂ to calculate column-average CO₂ VMR. This calculation eliminates errors which are common to both CO₂ and O₂ retrievals, such as errors in solar pointing and variation in solar intensity during interferogram acquisition, and allows useful retrievals to be obtained under partly cloudy conditions. Comparison of retrieved column O₂ to dry surface pressure during May 2004 – October 2005 shows linear agreement with a $2.27 \pm 0.25\%$ bias.

The column CO₂ retrievals were calibrated using aircraft profiles from the INTEx-NA and COBRA campaigns during summer 2004. The CO₂ 6228 cm⁻¹ and CO₂ 6348 cm⁻¹ band retrievals over-estimate the integrated aircraft profiles by factors of 1.0216 and 1.0240 respectively, with standard deviation of the fitting residuals of 0.39 ppmv and 0.42 ppmv. The systematic differences are attributed to known uncertainty in the CO₂ spectroscopic linestrengths and air-broadened width parameters. The comparison to aircraft integrated columns allows the CO₂ 6228 cm⁻¹ and CO₂ 6348 cm⁻¹ retrievals to be corrected to the accepted in situ calibration scale. The aircraft profiles were performed with the sun at airmass 1.1 – 2.0, and we are confident that our column-average CO₂ VMRs are now well-calibrated for these summertime, low airmass values. After calibration of the column retrievals with the integrated aircraft profiles and consideration of the complete error budget, we calculate the uncertainty in retrieved column-average CO₂ VMR to be ~0.3% (± 1.1 ppmv) at airmasses less than 2 (SZA less than 60 deg) throughout the measurement timeseries.

Acknowledgements

We thank Jeffrey Ayers for maintaining the ground-based FTS laboratory in Park Falls, Wisconsin. We thank Arlyn Andrews and the NOAA CCGG for providing WLEF Tall Tower CO₂ measurements. Bruce Daube thanks Victoria Chow and Bhaswar Sen for their support in obtaining the balloon CO₂ profile. We thank Andrew Orr-Ewing for helpful discussions and providing PGOPHER model results for the O₂ 7882 cm⁻¹ band. R.A.W. acknowledges support from the National Science Foundation and the California Institute of Technology. This work was funded by NASA Grant NAG5-12247 and NNG05-GD07G. Research at the Jet Propulsion Laboratory, California Institute of Technology is performed under contract with NASA.

Anderson, B. E., G. L. Gregory, J. E. Collins, G. W. Sachse, T. J. Conway, and G. P. Whiting (1996), Airborne observations of spatial and temporal variability of tropospheric carbon dioxide, *J. Geophys. Res.*, *101*, 1985-1997.

Bakwin, P. S., P. P. Tans, B. B. Stephens, S. C. Wofsy, C. Gerbig, and A. Grainger (2003), Strategies for measurement of atmospheric column means of carbon dioxide from aircraft using discrete sampling, *J. Geophys. Res.*, *108*, doi:10.1029/2002JD003306.

Bakwin, P. S., P. P. Tans, C. L. Zhao, W. Ussler, and E. Quesnell (1995), Measurements of carbon dioxide on a very tall tower, *Tellus*, *47*, 535-549.

Berger, B. W., K. J. Davis, C. X. Yi, P. S. Bakwin, and C. L. Zhao (2001), Long-term carbon dioxide fluxes from a very tall tower in a northern forest: Flux measurement methodology, *J. Atmos. Ocean. Tech.*, *18*, 529-542.

Brault, J. W. (1996), New approach to high-precision Fourier transform spectrometer design, *Appl. Opt.*, *35*, 2891-2896.

Cheah, S. L., Y. P. Lee, and J. F. Ogilvie (2000), Wavenumbers, strengths, widths and shifts with pressure of lines in four bands of gaseous $^{16}\text{O}_2$ in the systems $a^1\Delta_g - X^3\Sigma_g^-$ and $b^1\Sigma_g^+ - X^3\Sigma_g^-$, *J. Quant. Spectrosc. Radiat. Transfer*, *64*, 467-482.

Daube, B. C., K. A. Boering, A. E. Andrews, and S. C. Wofsy (2002), A high-precision fast-response airborne CO_2 analyzer for in situ sampling from the surface to the middle stratosphere, *J. Atmos. Ocean. Tech.*, *19*, 1532-1543.

Davis, K. J., P. S. Bakwin, C. X. Yi, B. W. Berger, C. L. Zhao, R. M. Teclaw, and J. G. Isebrands (2003), The annual cycles of CO_2 and H_2O exchange over a northern mixed forest as observed from a very tall tower, *Global Change Biology*, *9*, 1278-1293.

Denning, A. S., G. J. Collatz, C. G. Zhang, D. A. Randall, J. A. Berry, P. J. Sellers, G. D. Colello, and D. A. Dazlich (1996), Simulations of terrestrial carbon metabolism and atmospheric CO_2 in a general circulation model: 1. Surface carbon fluxes, *Tellus*, *48*, 521-542.

Dufour, E., F. M. Breon, and P. Peylin (2004), CO_2 column averaged mixing ratio from inversion of ground-based solar spectra, *J. Geophys. Res.*, *109*, doi:10.1029/2003JD004469.

GLOBALVIEW- CO_2 (2005), GLOBALVIEW- CO_2 : Cooperative Atmospheric Data Integration Project - Carbon Dioxide. CD-ROM, National Oceanic and Atmospheric Administration Climate Monitoring and Diagnostics Laboratory, Boulder, Colorado., edited.

Gloor, M., S. M. Fan, S. Pacala, and J. Sarmiento (2000), Optimal sampling of the atmosphere for purpose of inverse modeling: A model study, *Global Biogeochem. Cycles*, *14*, 407-428.

Gurney, K. R., R. M. Law, A. S. Denning, P. J. Rayner, D. Baker, P. Bousquet, L. Bruhwiler, Y. H. Chen, P. Ciais, S. Fan, I. Y. Fung, M. Gloor, M. Heimann, K. Higuchi, J. John, T. Maki, S. Maksyutov, K. Masarie, P. Peylin, M. Prather, B. C. Pak, J. Randerson, J. Sarmiento, S. Taguchi, T. Takahashi, and C. W. Yuen (2002), Towards robust regional estimates of CO_2 sources and sinks using atmospheric transport models, *Nature*, *415*, 626-630.

Komhyr, W. D., R. H. Gammon, T. B. Harris, L. S. Waterman, T. J. Conway, W. R. Taylor, and K. W. Thoning (1985), Global atmospheric CO_2 distribution and variations from 1968-1982 NOAA GMCC CO_2 flask sample data, *J. Geophys. Res.*, *90*, 5567-5596.

Kurylo, M. J., and S. Solomon (1990), Network for the Detection of Stratospheric Change, NASA Report, Code EEU.

Lafferty, W. J., A. M. Solodov, C. L. Lugez, and G. T. Fraser (1998), Rotational line strengths and self-pressure-broadening coefficients for the $1.27\text{-}\mu\text{m}$, $a^1\Delta_g - X^3\Sigma_g^-$, $v = 0-0$ band of O_2 , *Appl. Opt.*, *37*, 2264-2270.

Newman, S. M., I. C. Lane, A. J. Orr-Ewing, D. A. Newnham, and J. Ballard (1999), Integrated absorption intensity and Einstein coefficients for the O_2 $a^1\Delta_g - X^3\Sigma_g^-$ (0,0) transition: A comparison of cavity ringdown and high resolution Fourier transform spectroscopy with a long-path absorption cell, *J. Chem. Phys.*, *110*, 10749-10757.

Newman, S. M., A. J. Orr-Ewing, D. A. Newnham, and J. Ballard (2000), Temperature and pressure dependence of line widths and integrated absorption intensities for the O_2 $a^1\Delta_g - X^3\Sigma_g^-$ (0,0) transition, *J. Phys. Chem.*, *104*, 9467-9480.

Olsen, S. C., and J. T. Randerson (2004), Differences between surface and column atmospheric CO_2 and implications for carbon cycle research, *J. Geophys. Res.*, *109*, doi:10.1029/2003JD003968.

Rayner, P. J., I. G. Enting, R. J. Francey, and R. Langenfelds (1999), Reconstructing the recent carbon cycle from atmospheric CO_2 , $\delta^{13}C$ and O_2/N_2 observations, *Tellus*, *51*, 213-232.

Rayner, P. J., and D. M. O'Brien (2001), The utility of remotely sensed CO_2 concentration data in surface source inversions, *Geophys. Res. Lett.*, *28*, 175-178.

Rodgers, C. D., and B. J. Connor (2003), Intercomparison of remote sounding instruments, *J. Geophys. Res.*, *108*, doi:10.1029/2002JD002299.

Rothman, L. S., D. Jacquemart, A. Barbe, D. C. Benner, M. Birk, L. R. Brown, M. R. Carleer, C. Chackerian, K. Chance, L. H. Coudert, V. Dana, V. M. Devi, J. M. Flaud, R. R. Gamache, A. Goldman, J. M. Hartmann, K. W. Jucks, A. G. Maki, J. Y. Mandin, S. T. Massie, J. Orphal, A. Perrin, C. P. Rinsland, M. A. H. Smith, J. Tennyson, R. N. Tolchenov, R. A. Toth, J. Vander Auwera, P. Varanasi, and G. Wagner (2005), The HITRAN 2004 molecular spectroscopic database, *J. Quant. Spectrosc. Radiat. Transfer*, *96*, 139-204.

Smith, K. M., and D. A. Newnham (2000), Near-infrared absorption cross sections and integrated absorption intensities of molecular oxygen (O_2 , O_2-O_2 , and O_2-N_2), *J. Geophys. Res.*, *105*, 7383-7396.

Smith, K. M., D. A. Newnham, and R. G. Williams (2001), Collision-induced absorption of solar radiation in the atmosphere by molecular oxygen at 1.27 μm : Field observations and model calculations, *J. Geophys. Res.*, *106*, 7541-7552.

Tans, P. P., I. Y. Fung, and T. Takahashi (1990), Observational constraints on the global atmospheric CO_2 budget, *Science*, *247*, 1431-1438.

Vay, S. A., J. H. Woo, B. E. Anderson, K. L. Thornhill, D. R. Blake, D. J. Westberg, C. M. Kiley, M. A. Avery, G. W. Sachse, D. G. Streets, Y. Tsutsumi, and S. R. Nolf (2003), Influence of regional-scale anthropogenic emissions on CO_2 distributions over the western North Pacific, *J. Geophys. Res.*, *108*, doi:10.1029/2002JD003094.

Warneke, T., Z. Yang, S. Olsen, S. Korner, J. Notholt, G. C. Toon, V. Velazco, A. Schulz, and O. Schrems (2005), Seasonal and latitudinal variations of column averaged volume-mixing ratios of atmospheric CO_2 , *Geophys. Res. Lett.*, *32*, doi:10.1029/2004GL021597.

Yang, Z., P. O. Wennberg, R. P. Cageao, T. J. Pongetti, G. C. Toon, and S. P. Sander (2005), Ground-based photon path measurements from solar absorption spectra of the O_2 A-band, *J. Quant. Spectrosc. Radiat. Transfer*, *90*, 309-321.

Yang, Z. H., G. C. Toon, J. S. Margolis, and P. O. Wennberg (2002), Atmospheric CO_2 retrieved from ground-based near IR solar spectra, *Geophys. Res. Lett.*, *29*, doi:10.1029/2001GL014537.

Zhao, C. L., P. S. Bakwin, and P. P. Tans (1997), A design for unattended monitoring of carbon dioxide on a very tall tower, *J. Atmos. Ocean. Tech.*, *14*, 1139-1145.

Figure 1. (a) Photograph of the automated FTS laboratory located 25 m south of the WLEF Tall Tower. A dome, weather station, and network camera are mounted on the roof. (b) Block diagram showing the laboratory. A servo-controlled solar tracker directs the solar beam through a CaF_2 window to the Bruker 125HR spectrometer in the laboratory. A 10 cm cell with 5.1 hPa HCl is mounted in the source compartment of the 125HR, prior to the input field stop. Two detectors simultaneously record the solar spectrum in the $3,900 - 15,500 \text{ cm}^{-1}$ region. The Hercules computer uses custom data acquisition software to monitor and control the 125HR spectrometer, solar tracker, dome, weather station, camera, scroll pump, GPS satellite time server, temperature sensors, and heaters.

Figure 2. (a) A single spectrum recorded on 9 Sep 2004, with 0.014 cm^{-1} resolution. Signal to noise ratio is ~ 900 for the InGaAs detector and ~ 500 for the Si diode detector. Near-infrared absorptions by H_2O , O_2 , CO_2 , CH_4 , CO , and N_2O are labeled with black bars. (b) An enlarged view of the same spectrum, demonstrating the resolution and signal to noise in a region with strong CO_2 lines.

Figure 3. (a) Relationship between retrieved column O_2 and dry surface pressure for spectra recorded at airmasses between 2 and 3. The retrieved column O_2 has been reduced by 1.0227. Dry surface pressure is the measured surface pressure converted to a column density minus the retrieved H_2O column. (b) Time series of column-average O_2 VMR during May 2004 – Oct 2005. Scatter is attributed to error in the linestrengths and air-broadened widths which cause the O_2 retrievals to vary with temperature and airmass. The systematic changes of O_2 VMR over time are attributed to detector non-linearity.

Figure 4. Spectral retrievals compared for a clear day (14 Aug 2004) and a partly cloudy day (15 Aug 2004). (a) Column CO₂ retrieved from the 6228 cm⁻¹ (black) and 6348 cm⁻¹ (gray) bands. Although the retrievals demonstrate precision of ~0.1%, there is a systematic offset of ~0.2% between the two bands. This offset is attributed to errors in the CO₂ linelist parameters. (b) Column O₂ retrieved from the 7882 cm⁻¹ band. (c) Column-average CO₂ VMR calculated from column CO₂ / dry surface pressure. (d) Column-average CO₂ VMR calculated from $0.2095 \times \text{column CO}_2 / \text{column O}_2$.

Figure 5. (a) Ground track of the NASA DC-8 during a vertical profile from 0.7 – 10.0 km on 12 Jul 2004. The location of the Wisconsin Tall Tower is indicated. Aircraft altitude is shown, with black = 0.7 km and light grey = 12 km. (b) In situ CO₂ measured during the 12 Jul 2004 profile.

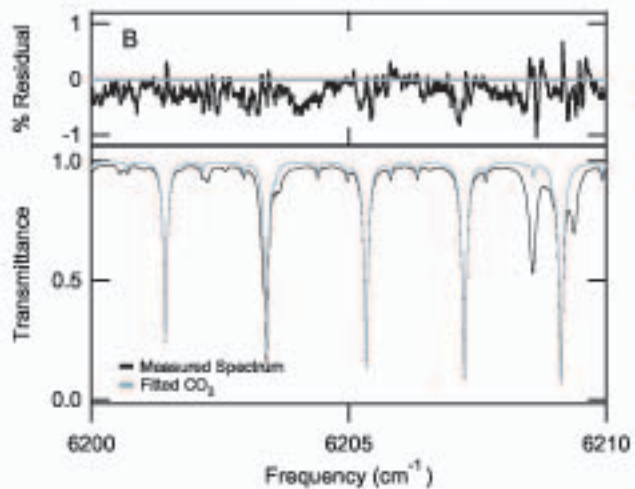
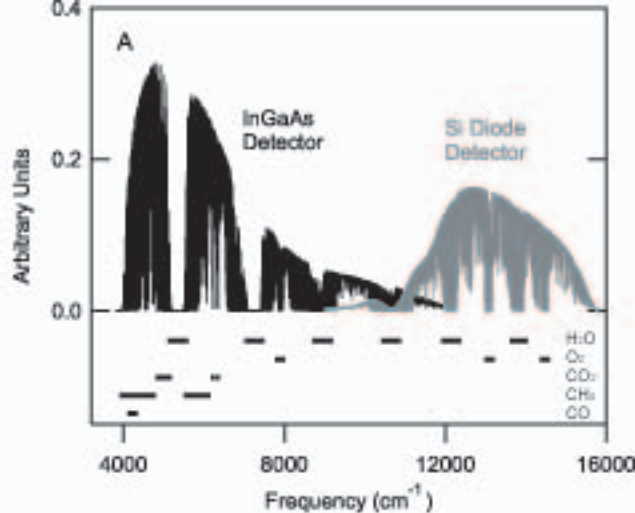
Tropopause pressure is determined from the NOAA CDC reanalysis. Above the aircraft ceiling (10.0 km), the median measured free tropospheric CO₂ value is assumed to extend to the tropopause.

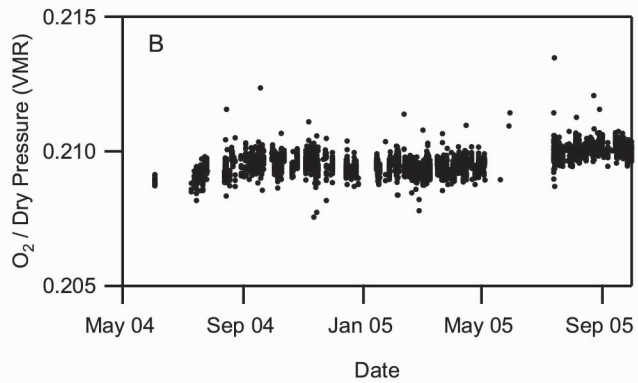
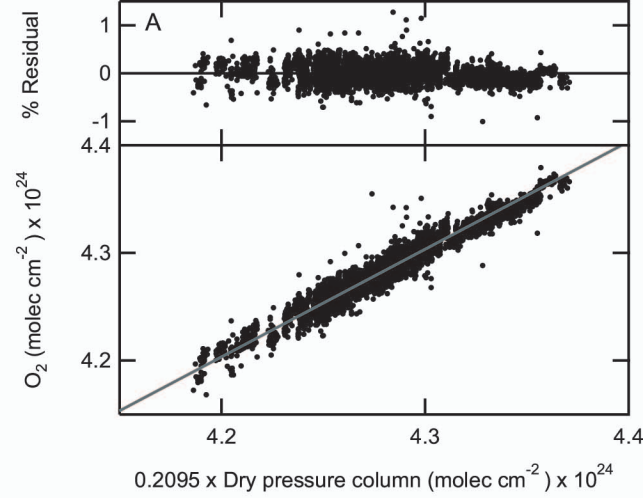
Above the tropopause, the assumed CO₂ profile is taken from a Sept 2004 balloon profile from 35 N, 104 W. The CO₂ profile is integrated with respect to pressure to calculate the total column. (c) Averaging kernel for the FTS CO₂ retrievals. (d) Column-averaged CO₂ VMR for FTS spectra recorded during the aircraft profile. CO₂ 6228 cm⁻¹ band retrievals shown in black; CO₂ 6348 cm⁻¹ band retrievals shown in gray. Intermittent clouds prevented continuous data acquisition.

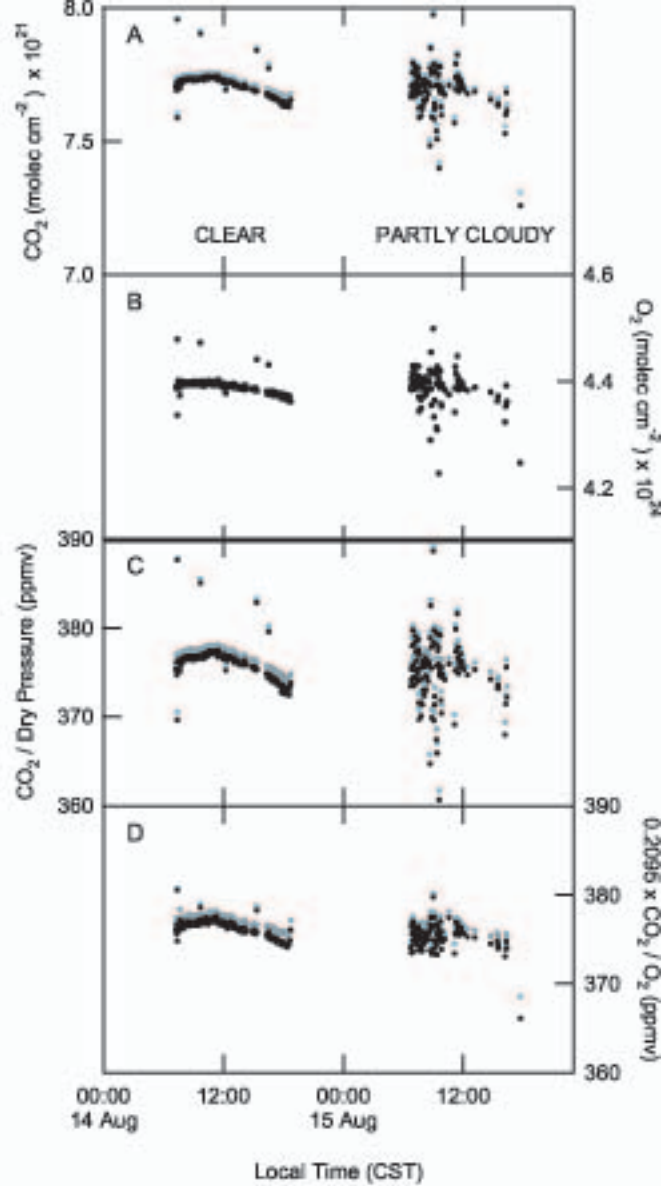
Figure 6. Integrated profiles by the DC-8 (triangles) and King Air (circles) compared to FTS retrievals from the two CO₂ bands. CO₂ 6228 cm⁻¹ band retrievals shown in black; CO₂ 6348 cm⁻¹ band retrievals shown in gray. Each integrated aircraft profile has been divided by the dry surface pressure, yielding the familiar units of ppmv. The relationship between integrated profile and FTS column-average CO₂ VMR is linear for each band. A linear fit with intercept 0 gives slopes of

1.0216 for the CO₂ 6228 cm⁻¹ band and 1.0240 for the CO₂ 6348 cm⁻¹ band. The upper panel shows the difference between the FTS measurements and the fitted line.

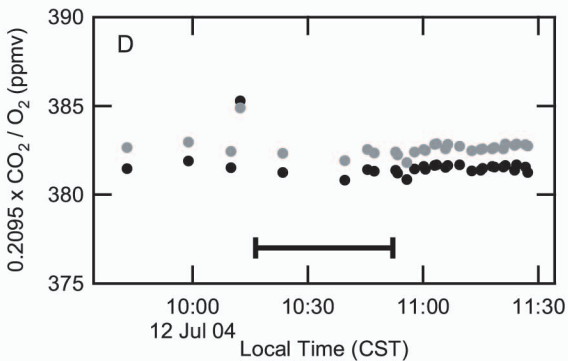
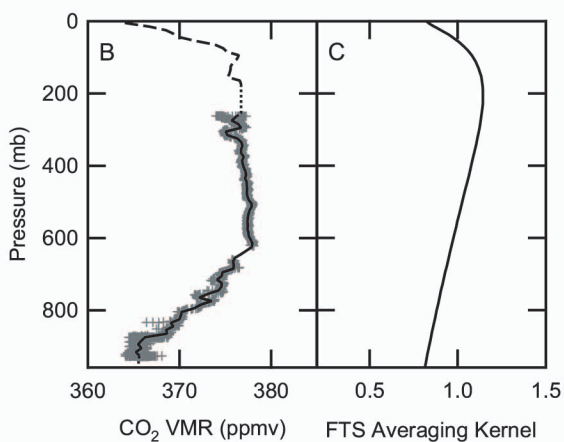
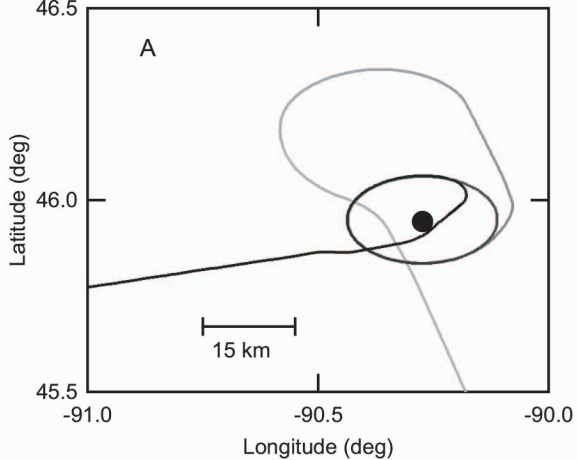
Figure 7. (a) Diurnal variation of column-average CO₂ VMR (black symbols) and Tall Tower CO₂ at 30-m (black line) and 396-m (grey line). (b) Seasonal cycle of column-average CO₂ VMR (black symbols) and Tall Tower CO₂ (grey symbols) during May 2004 – Oct 2005. Tall Tower CO₂ at 396-m is shown as daily averages between 10:00 – 14:00 CST. Column-average CO₂ VMR is shown as daily averages for airmasses 2 – 4 (SZA 60 – 75 deg).

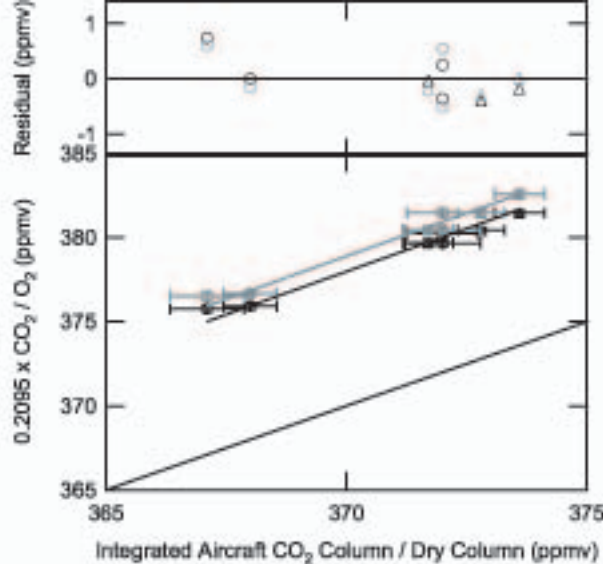




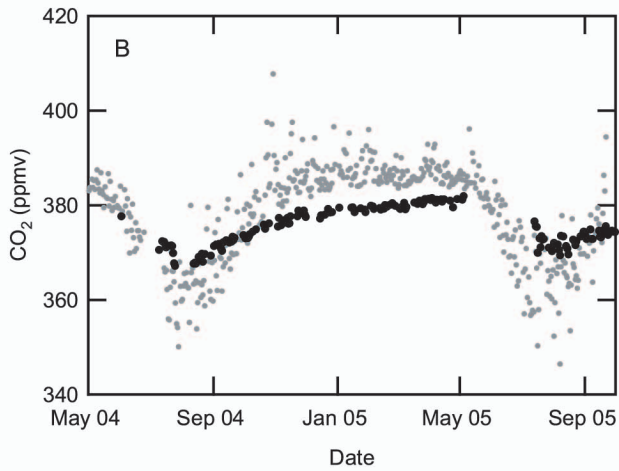
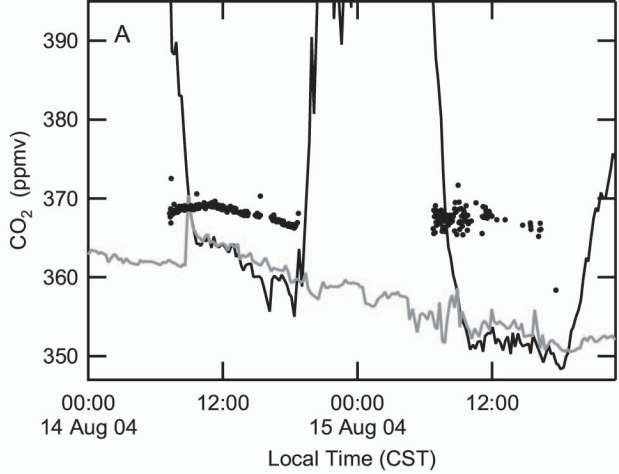


Washenfelter et al. (2006JD007154)
Figure 4





Washenfelder et al. (2006JD007154)
Figure 6



Washenfelter et al. (2006JD007154)
Figure 7